Express Polymer Letters Vol.18, No.9 (2024) 883–900
Available online at www.expresspolymlett.com
https://doi.org/10.3144/expresspolymlett.2024.66

Research article

Thermo-mechanical characterisation of polycarbonate-based sheet moulded composites fabricated from off-cut waste unidirectional tapes

Chethan Savandaiah[1,2*], *Andreas Kapshammer*[3], *Bernhard Plank*[4], *Vanja Stolcer*[2], *Christian Marschik*[1], *Zoltan Major*[3]

[1]Competence Centre CHASE GmbH, 4040-Linz, Austria
[2]Wood K Plus-Kompetenzzentrum Holz GmbH, 4040-Linz, Austria
[3]Institute of Polymer Product Engineering, Johannes Kepler University, 4040-Linz, Austria
[4]Research Group Computed Tomography, University of Applied Sciences Upper Austria, 4600 Wels, Austria

Received 13 March 2024; accepted in revised form 5 June 2024

Abstract. Thermoplastic (TP) composites, known for their ease of handling, suitability for high production rates, and recyclability, are emerging as a promising alternative to thermoset-based composites. The expected growth in TP-based composites in automotive, sports, and aerospace industries may result in increased post industrial waste. To address this, we repurposed our in-house process scrapped carbon fibre-reinforced polycarbonate tapes into sheet moulding compounds (SMCs) and Hybridised SMCs (Hy-SMCs) using compression moulding. In Hy-SMCs, the top and bottom layers were unidirectional tapes, while the core section had randomly oriented platelets in a 50:50 ratio. Our evaluation included qualitative and thermo-mechanical standard tests. The incorporation of unidirectional tapes in Hy-SMCs significantly improved the tensile and flexural properties of SMCs. Specifically, these enhancements resulted in an impressive 81 to 85% increase in mechanical strength compared to the standard aluminium grade. Additionally, Hy-SMCs exhibited a 120 to 130% increase in tensile and flexural properties compared to SMCs. Fractography revealed a complex relation between fractured surfaces, with multimode failures in both SMCs and Hy-SMCs. Also, the non-destructive evaluation showed platelet reorientation during consolidation and localised voids with increased specimen thickness.

Keywords: *thermoplastic composites, carbon fibre, polycarbonate, sheet moulding compounds*

1. Introduction

Thermoplastic (TP) based composites are a type of advanced composite material poised to play an increasingly significant role in aerospace, automotive, sports and construction industries alike due to the ease of handling and storage, efficiency and cost-effective scalability. Also, it is well suited for high-volume production rates and exhibits improved impact strength, low flame-smoke toxicity and chemical resistance [1]. The TP composite application avenues are increasing, so are the invariable non-conforming and off cut wastage during die-cutting of composite tapes used for conventional processing techniques such as injection moulding and compression moulding. Every so often, processed wastes are repurposed to fabricate quasi-isotropic compression pressed plates for further processing into a complex shaped part, trending towards closed-loop circularity [2]. Seemingly, several research has been published to assess the product life of composites and the recycling of composite materials using state-of-the-art evaluation and decision-making tools such as life cycle assessment and life cycle impact assessment. In all instances, recycling and reprocessing [3] have

*Corresponding author, e-mail: c.savandaiah@wood-kplus.at

proven beneficial compared to downcycling, landfill and incineration [4–6].

Kiss *et al*. [2], investigated the recyclability and thermo-mechanical performance of carbon fibre-reinforced polyamide 6 and glass fibre-reinforced polypropylene laminates. They achieved this by shredding and compression moulding the materials into randomly oriented sheet moulded compounds (SMCs). SMCs fabricated from shredded fibres (0.5–7 mm, 4 mm sieve) and (5–25 mm, 8 mm sieve) showed inferior thermo-mechanical performance compared to standard injection moulded specimens. Researchers inferred the poor mechanical performance of SMCs was due to increased fibre length attrition and short fibre randomised orientation during fabrication. Similarly, Eguémann and coworkers [7, 8] and Roux *et al*. [9] investigated the role of recyclability and fibre lengths in polyether ether ketone (PEEK) SMC door hinges performance compared to hinges produced by aerospace grade steel. It was reported that recycled SMC hinges exhibited a greater ultimate load-carrying ability before failure when compared to injection moulded composite hinges. Additionally, fibres 10 mm in length were found to be suitable for processing and could potentially replace steel door hinges, in contrast to the fibres 20 mm in length. Furthermore, within the TPC-Cycle Project, TenCate Advanced Composites incorporated continuous fibre material with recycled SMCs and achieved a greater degree of freedom in designing composite parts and processing. The hybridisation of composite material allowed the moulding of stiffening ribs with variable thickness across the part and bosses around the holes, which is difficult to achieve using just continuous fibrous material [10]. Similarly, Trauth and Weidenmann [11], performed hybridisation of continuous-discontinuous glass/carbon fibre SMCs and achieved a significant increase in tensile (171%) and compressive modulus (151%) properties compared to corresponding SMCs specimens.

The carbon fibre-reinforced polycarbonate (PC) matrix composites have better chemical inertness and environmental degradation resistance and exhibit better fatigue resistance compared to thermoset (TS) based composites. To the best of our knowledge, very few articles have examined the thermo-mechanical properties and qualitative performance of the PC based composites [12, 13] and none for PC based SMCs. In-house trial runs generated approximately 20–25% off-cuts and process-scraped unidirectional (UD) carbon fibre-reinforced PC composite tapes. However, process-scraped off-cuts and non-conforming UD composite tapes may exhibit properties similar to pristine composite tapes. Additionally, the thermo-mechanical properties of the composite are significantly influenced by the fibre length. Therefore, based on the literature study, we decided to maintain the platelet lengths between 25 and 50 mm [14, 15]. Henceforth, the underscored potential of the TP-based SMCs as a suitable replacement for TS-based SMCs, we decided to repurpose our internal process scraps. We achieved this by utilising compression moulding to fabricate high quality, randomly oriented and hybridised randomly oriented long carbon fibre-reinforced PC platelets' composites having different thicknesses.

In our current research, we tried to address the influence of processing technique on PC based SMCs Hy-SMCs. The fabricated composite plates were subjected to qualitative and thermo-mechanical standard tests' methodology to determine the processability and material. We characterised SMCs specimens using X-ray computed tomography, heat deflection temperature, and fractography with digital microscopy and scanning electron microscopy to assess the quality. To evaluate the thermo-mechanical properties specimens were subjected to standard short beam strength, tensile, flexural, notched Charpy impact, and dynamic mechanical thermal analysis tests. The qualitative and thermomechanical data reported in the current research work may be beneficial in computer aided engineering. The outcome of the results may be further studied to optimise the performance and processing conditions to produce different grades of SMCs.

2. Materials and methods

2.1. Materials

Process scrapped and non-conforming, carbon fibre-reinforced PC matrix based UD tapes were sheared using a generic desktop sized paper cutting device (Figure 1). The composite UD tape has a density of 1.5 g·cm^{-3} with a measured thickness of 0.17–0.18 mm and a carbon fibre content between 50–53 wt%. The length and width of the platelets depended on the area of the scrapped tapes, *i.e.* scrapped off-cuts and contour-cut UD tape dimensions. The average platelets length was maintained between 25–50 mm, and varying width up to 25 mm. Similarly, non-conforming UD tapes were utilised to

produce hybridised SMCs (Hy-SMCs) and UD tapes in the top and bottom layers with SMC cores in a 50:50 ratio, respectively.

2.2. Compression moulding of SMCs and hybrid SMCs plates

The process scrapped are non-conforming UD and contour-cut tapes rejected by automated optical contour recognition software for pick and place robotic system [16]. Compression moulding of SMC plates was performed based on the bulk moulding technique, as shown in Figure 1. The consolidation unit Baugroesse 2 produced by FILL GmbH, Gurten, Austria, consists of two compressing presses with a usable area of 860×360 mm (length × width) each, and a maximum closing force rating of 24 kN (melting) and 310 kN (consolidation). For lab-scale trials, the first stage involves cutting of process scrapped and off cut tapes into platelets. Initially, a desktop sized cutting device is utilised but for large-scale industries, more efficient shearing machineries are commercially available. Furthermore, before compression moulding, the platelets and UD tapes are pre-dried inside a vacuum chamber (Binder VD53) at 120 °C for 60 min. After drying, the platelets were weighed according to the volume of SMCs and Hy-SMCs plates (see Table 1), and vacuum sealed in individual bags. The detailed thermocouple study of the melting- and consolidation cycles are shown in Figure 2. The pre-dried platelets were manually filled into the tool cavity, and compression moulded at 325 °C with an applied compression pressure of 3.4 bar for 180 s. After the melting cycle, the molten mass is transferred onto the adjacent consolidation press maintained at 100 °C followed by applied compression pressure of 47.1 bar for 180 s. At the end of the solidification cycle, SMC plates are manually extracted for further processing. Similarly, the Hy-SMCs are produced by placing non-conforming 0.17–0.18 mm thick UD tape stacks in the top and bottom of the cavity and filling the core (middle) with process scrapped platelets.

Table 1. Compression-pressed SMCs and Hy-SMCs plates dimensions.

Nature of plates	Plate dimensions, l×w×t* [mm]	SMCs [wt%]	UD-tapes [wt%]
SMCs	230×150×2	100	–
SMCs	220×130×3.4	100	–
SMCs	160×110×4	100	–
Hy-SMCs	220×130×3.4	50	50
Hy-SMCs	160×110×4	50	50

*l – length, w – width, t – thickness.

The process settings for fabricating the SMCs tabulated in Table 2 were selected according to Birtha *et al*. [17]. To validate the chosen conditions viability to the selected plates dimensions (Table 1), we followed the experimental procedure detailed by Kobler *et al*. [18]. Therefore, a thermocouple wire (type-K) was fixed in the middle (core) section of a 2 mm thick UD-tape stacked specimen to evaluate the feasibility of the selected processing settings and conditions for the consolidation unit. The data acquisition system QuantumX, produced by Hottinger, Brüel & Kjær GmbH, Darmstadt, Germany, recorded the core temperature and applied pressure during processing at 10 and 300 Hz, respectively. In Figure 2, prior to placing the specimen with thermocouple

Table 2. Processing settings are used to prepare SMCs and Hy-SMCs.

Consolidation unit	Temperature [°C]	Pressure [bar]	Cycle time [s]
Melting press	325	3.4	180
Consolidation press	100	47.1	180

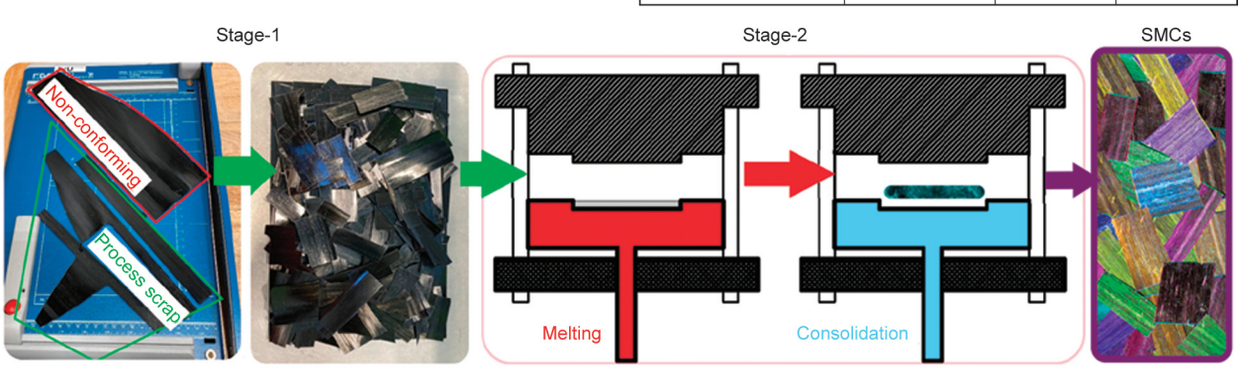

Figure 1. Different stages in the preparation of sheet moulded compounds (SMCs) plates. Stage-1 involves preparation of platelets and filling the tool cavity, stage-2 involves melting of platelets into a mass, followed by consolidation of the melt to form a solid SMCs plate.

wire, the tools were subjected to cyclic pressure temperature process, and thus the recorded specimen temperature increased directly after transferring it into the tool (black dotted line-Specimen load). The melting cycle starts when the 90% of set pressure value (red solid line) is reached and it is sustained until the end of cycle (180 s). Subsequently, the specimen inside the tool contacts the heated platens, which triggers the temperature ramp (red dash-dot-dash line). Furthermore, at the end of the melting cycle, the set temperature reached the core of the specimen, and this signifies the selected cycle time is sufficient. The molten specimen inside the platen is then transferred (15 s) onto the consolidation press automatically by a shuttle system. Similarly, the consolidation cycle starts when 90% of the set pressure value is reached (solid blue line) and is maintained until the end of the cycle; the decline in specimens' core temperature (blue dashed line) is also recorded. The foremost important parameter during consolidation is the applied pressure, and the set value (47.5 bar) is reached well before the onset of glass transition temperature (T_g). Also, the recorded core temperature of the consolidated specimen reached the set temperature (100 °C) well within the set cycle time (180 s). For more information on the compression pressing setup, please follow the experimental section of Birtha *et al*. [17].

2.3. Mechanical tests

All specimens were prepared according to the corresponding standard using Mutronic DIADISC 4200 precision cut-off saw, produced by Mutronic GmbH & Co KG, Rieden am forggensee, Germany. Before testing, all the standard specimens were stored in the standard control cabinet as per ASTM D618-00 (relative humidity of 50% at 23 °C for 72 h).

Interlaminar shear strength (ILSS) was determined according to ASTM 2344/D 2344M-00^{e1} standard test method. The MTS 852 test damper system (MTS Systems Corporation, Eden Prairie, Minnesota, USA) was equipped with a 10 kN load cell and axial movement was recorded. The specimen dimension of 25×6.4×2 mm (l×w×t) was used, the span length was adjusted to span to thickness ratio of four, and the testing speed was set to 1 mm·min^{-1}. The specimens with only mid-plane interlaminar shear failure were considered for evaluation and test results were evaluated to a significance level of 5%. The identification of the failure type and region was determined using a TOOLCRAFT 1713197 digital microscope (Conrad Electronic SE, Hirschau, Germany) having a native resolution of 3072×1728 pixels with a maximum focus range of 50 mm and 300× optical zooming capability. Out of fifteen tested specimens, only ten were evaluated to a significance level of 5%.

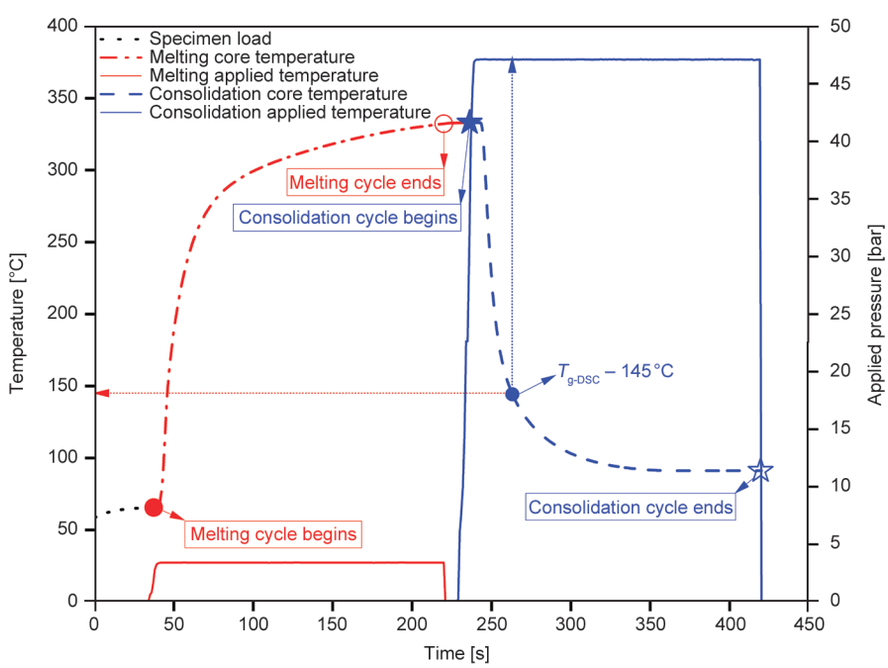

Figure 2. Thermocouple study of compression pressed UD plate (2 mm), temperature and applied pressure as a function of time. Solid lines with corresponding colour codes indicate the recorded applied force for each cycle. The recorded melting cycle temperature ramp is represented by red dash dot dash line and the temperature decline during consolidation cycle represented by blue dashed line. Glass transition ($T_{g\text{-}DSC}$) temperature was determined using differential scanning calorimetry.

The tensile properties of the SMCs and Hy-SMCs were determined using the ISO 527-4/ 2/ 2 standard test method. The specimen dimension of 220×25×3.4 mm, with grip to grip separation of 100 mm. The Zwick/Roell Z150 (ZwickRoell GmbH & Co. KG, Ulm, Germany) equipped with a 150 kN load cell and macro extensometer were utilised for testing. The modulus of elasticity was determined between 0.05 and 0.25% at a constant testing speed of 2 mm·min^{-1}. For SMCs specimens' emery cloth was used, and glass fibre-reinforced composite end tabs for Hy-SMCs (Figure 3). A total of five specimens for each type were assessed, and the test results were evaluated at a significance level of 5%.

To distribute stress concentration over larger area and achieve pure bending phenomenon during tests, four point bending (4PB) based flexural properties of SMCs and Hy-SMCs were determined based on ISO 14125:1998 Class II standard method (Figure 3). The Zwick/Roell ZMART.PRO (ZwickRoell GmbH & Co. KG, Ulm, Germany) equipped with a 10 kN load cell was used for 4PB tests of five specimens (80×15×4 mm) for each type at 2 mm·min^{-1}, and results were evaluated to a significance level of 5%.

The notched Charpy impact specimens were prepared according to EN ISO 179-1-(1/e/A) standard test method. A wedge-shaped cutting blade with a notch depth of 2 mm and a tip radius of 0.25 mm was used to create a notch on SMCs and Hy-SMCs standard specimens (80×10×4 mm). Instron CEAST 9050 Impactor II (Instron GmbH, Darmstadt, Germany) with 8 J pendulum was used for measuring the impact energies and impact strength of specimens, and the obtained values were evaluated to a significance level of 5%.

2.4. Heat deflection temperature

As with any machined part, it is critical for a designer to predict material behaviour subjected to elevated temperature and strain. Cutting and drilling tools produce frictional heat when they encounter TP-based composites, and TP tend to deform under high temperature. To fabricate composite products with accurate dimensions and tolerances, it is important to understand the HDT of a TP matrix material. Also, it is an important parameter of design consideration for injection moulding processes, increased HDT leads to reduced processing cycle time. The heat deflection

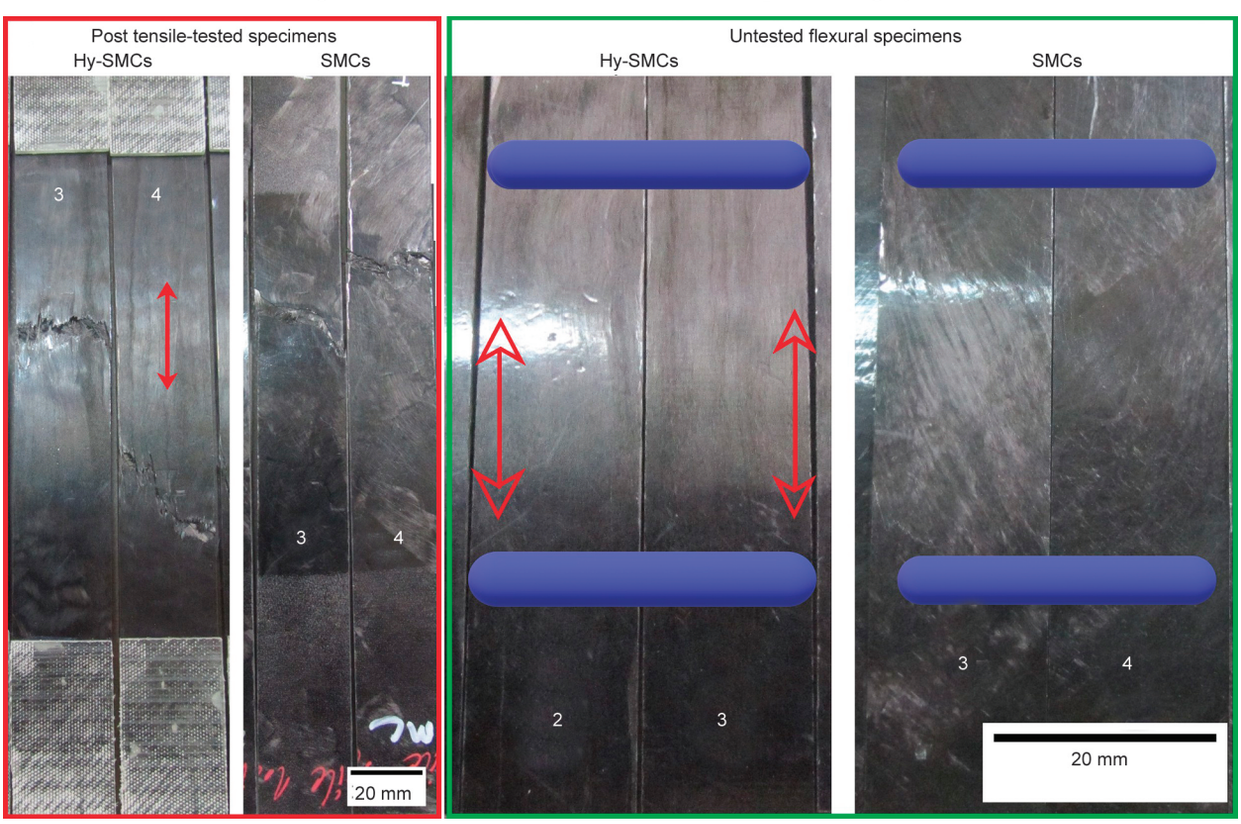

Figure 3. Post tensile tested Hy-SMCs with glass fibre tabs and SMCs with emery cloth (faint white scratches). The red arrow indicates top and bottom layers fibre direction in Hy-SMCs. For untested flexural specimens, flexural loading is indicated by blue pins.

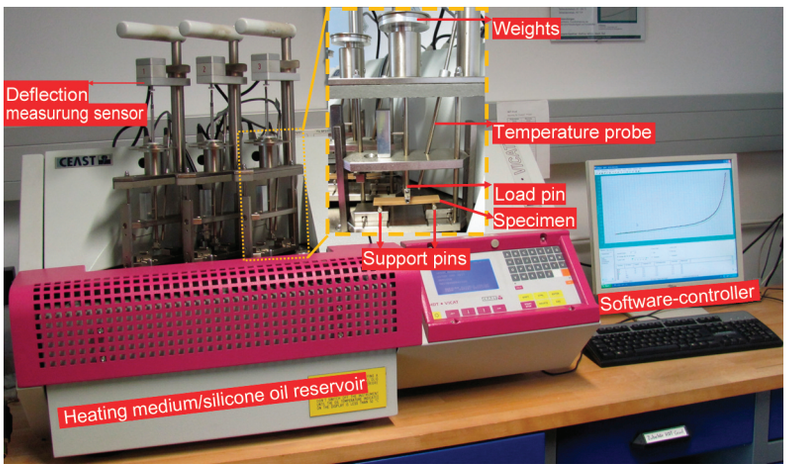

Figure 4. Photography of standard heat deflection temperature measuring device showing different points of interest and specimen holder setup in the inset.

temperature (HDT) testing was performed according to EN ISO 75 in HDT-B (0.45 MPa and 120 °C·h^{-1}) and HDT-C (8 MPa and 120 °C·h^{-1}) modes for specimens having 80×10×4 mm dimensions. In Figure 4, the measurements were conducted in Instron CEAST HV 3 (Instron GmbH, Darmstadt, Germany) and silicon oil was used as a heating medium, so the maximum measured temperature is 200 °C. The testing is stopped at the set maximum deflection and the temperature is recorded for each specimen.

2.5. Dynamic mechanical thermal analysis (DMTA)

The thermo-mechanical properties of SMCs and Hy-SMCs were investigated using the Netzsch GABO Eplexor 500 N testing machine (Netzsch GmbH & Co. KG, Selb, Germany). The orientation of the outer UD region for the Hy SMC specimen was aligned with the deflection curve of the test setup. The temperature sweep measurements were performed on 50×10×3.4 mm specimens in three-point bending mode with a support length of 20 mm, from 30 up to 210 °C at a heating rate of 3 K·min^{-1} and a corresponding step width of 3 °C. At each interval, a soaking time of 60 s was set to achieve a homogenous temperature distribution within the sample. Due to a displacement-controlled loading, a sinusoidal deflection of 30 µm was applied for forty intervals at a frequency of 1 Hz after a contact force of 0.5 N was reached. The mechanical and thermo-mechanical tests utilised to evaluate material responses of SMCs and Hy-SMCs are tabulated in Table 3.

Table 3. Details of SMCs and Hy-SMCs specimens subjected to different test methods.

Nature of plates (thickness)	Test method
SMCs (2 mm)	ILSS, DMTA
SMCs (3.4 mm)	Tensile, DMTA
SMCs (4 mm)	Flexural (4PB), Notched Charpy impact test, HDT
Hy-SMCs (3.4 mm)	Tensile, DMTA
Hy-SMCs (4 mm)	Flexural (4PB), Notched Charpy impact test, HDT

2.6. X-ray computed tomography and scanning electron microscope

A non-destructive technique, X-ray computed tomography (XCT), was employed to determine the fibre orientation, fractography, and part quality (see Figure 5). XCT scans were conducted on both tested and untested specimens. XCT scans (fractography) of tested and region of interest (ROI) high-resolution XCT scans for untested specimens were performed with a Nanotom 180NF (GE Sensing & Inspection Technologies GmbH, Wunstorf, Germany). The 180 kV sub focus X-ray tube was equipped with a molybdenum target on a beryllium window. A 2304×2304 pixel flat panel detector (Hamamatsu Photonics K.K., Shizuoka, Japan) was used as the detector. Based on the specimen area, platelets' length and to reduce measurement effort, the used voxel size was set between 2.7 and 31 µm^3. A multiscale approach was applied to optimise the segmentation results of matrix-rich areas and the fibre orientation distribution analysis as described by Stelzer *et al*. [19]. Similarly, the void volume fraction was determined by a multiscale approach according to the procedure specified by Plank and co-workers [20, 21]. Therefore, additional ROI high-resolution

scans at 2.7 µm^3 voxel size were performed on untested specimens, and an ISO 48 threshold for a grey value-based segmentation was determined for specimens scanned with a voxel size of 10.5 µm^3. It must be noticed that the use of a global threshold always represents a compromise between an under- and over-segmentation of void structures. For void volume fraction calculations, only structures bigger than 8 connected voxels were considered to minimise-mis-segmentation of smaller artefacts and image noise. Whereas the CT void volume fraction is calculated as the ratio between "segmented voxels" divided by "total number of voxels" in a defined "region of interest". Detailed parameters and the resulting voxel size for the test setup are listed in Table 4.

Reconstruction of XCT scanned specimen were done using datos-x software, based on the filtered back projection algorithm, provided by the XCT manufacturer. During reconstruction, a software-based beam hardening correction (value 8) for multi-materials was applied. For voxel dataset handling, manual- and semiautomatic registration of individual scans, VGSTUDIO MAX 3.3 (Volume Graphics GmbH, Heidelberg, Germany) was used as a standard software tool. Additional fibre orientation analysis was done using the fibre composite material analysis tool. The following main parameters were used in VGSTUDIO MAX on a quadratic ROI of 9.8×0.8 mm: mode fibres (direction); scale-1, integration radius-2, and plane projection 0-1-0. Furthermore, to get a fibre orientation distribution over the entire specimen thickness, integration mesh cells of 100 µm thickness were evaluated.

The fractography of the impact-tested notched Charpy samples was investigated under a scanning electron microscope (SEM) with accelerating voltage at 10 kV using Phenom Pro X by ThermoFisher Scientific Inc., Massachusetts, USA. For qualitative spatial resolution, the fractured surface was sputtered with very thin conductive gold coating (15 nm) in SC7620 Mini sputter from Quorum technologies, Laughton village, UK, for 100 s at 20 mA.

3. Result and discussion

3.1. Fibre orientation and void volume fraction

SMCs are susceptible to localised structural weaknesses in-plane, highly anisotropic platelets fabricated

Table 4. Detailed XCT parameters and applied voxel size for the experimental test setup.

Voxel size [µm^3]	Tube voltage [kV]	Tube current [µA]	Number of projections	Average/skip	Detector integration time [ms]	Total scanning time [min]
2.7	60	200	1800	8/2	500	153
7.5	60	160	1800	6/1	700	150
10.5	60	200	1700	8/2	500	145
16.0	60	280	1800	7/2	500	135
31.0	60	425	1700	6/1	800	162

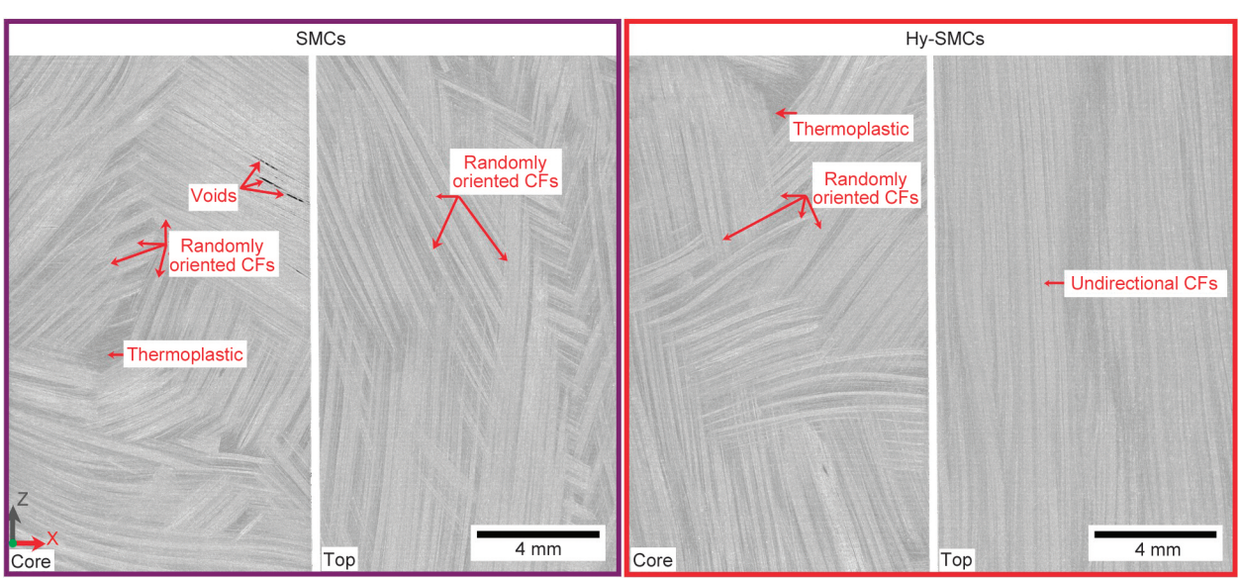

Figure 5. Exemplary XCT cross-sectional images detailing sectional difference between SMCs and Hy-SMCs. Light grey corresponds to carbon fibres, dark grey is polycarbonate, and voids are identifiable from black colour.

into randomly oriented laminates double-down as a localised flaw within the laminate when fibres are out-of a plane to the applied load [22, 23]. Hence, XCT is a helpful tool in understanding the influence of the fabrication process on platelet orientation and quality. In Figure 6, the random fibre orientations are vividly revealed as the projected angle on SMCs and Hy-SMCs XCT sectional images. The composite platelets laminate is shown with scalar field's colour scales for the randomised orientation in SMCs, the core region of Hy-SMCs, and primarily UD-oriented carbon fibres in the top and bottom layers of Hy-SMCs. The initial platelet orientation and the optimised processing conditions resulted in a highly randomised fibre orientation in 2 mm thick SMC plates, in contrast to the more aligned fibres found in the 3.4 and 4 mm thick SMC plates. Furthermore, 3.4 and 4 mm thick SMCs scalar field's colours exhibit most platelets' layers having fibre orientation between 30°–60° projected angle. Similarly, the core of the Hy-SMCs (3.4 and 4 mm) has randomly oriented platelets, whereas the higher randomly oriented platelets are formed in 4 mm (aligned between 0°–180°) compared to 3.4 mm (aligned at 50° and 150°). Additionally, the partial re-orientation of UD composite tapes in Hy-SMCs (90°–120°) is due to

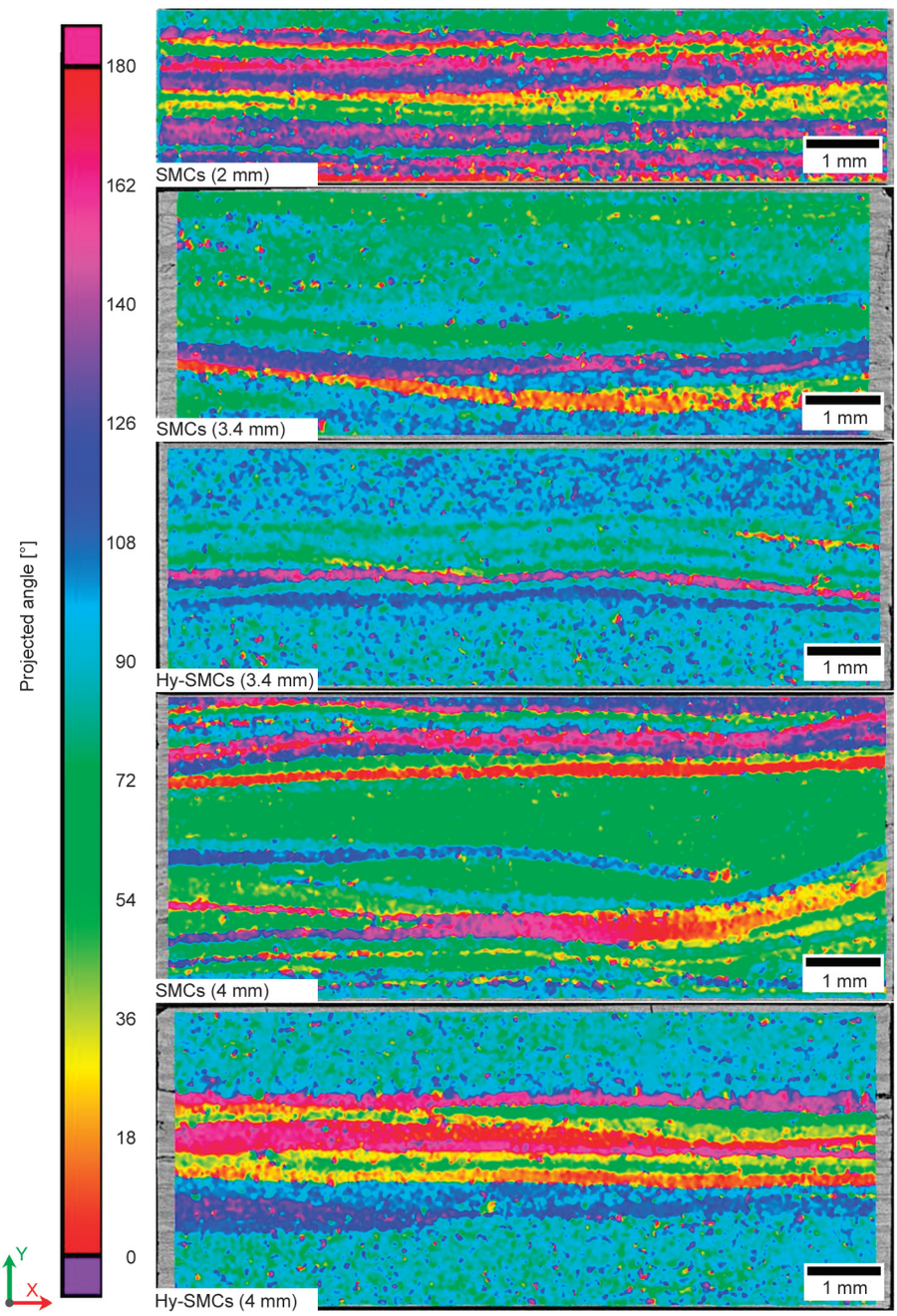

Figure 6. XCT cross-sectional images of SMCs and Hy-SMCs are shown as projected angles with scalar colour field's scale.

process-induced undulation and is influenced by the flow of high-viscous matrix melt subjected to high compaction pressure; similar results were also reported by Belliveau and co-workers [24, 25].

Similarly, XCT is also used to identify and quantify the voids as it is necessary to assess the quality of the fabricated platelets' laminate via non-destructive methodology. The void volume fraction of each specimen type of SMCs and Hy-SMCs are tabulated in Table 5, and localised void percentages over the individual specimen thickness are depicted in Figure 7. The quantified void volume fraction and void percentage of SMCs (2 mm) are imperceptible when compared to thicker specimens, and this may be attributed to optimised fabrication conditions and specimen thickness. Similarly, the measured void volume fraction of Hy-SMCs (3.4 mm) is like SMCs (2 mm), a localised minor void content (0.6 vol%). The thicker SMCs (3.4 and 4 mm) and Hy-SMCs (4 mm) have similar void volume fractions and are well within acceptable industrial standards of less than 2 vol% [26], but they have different localised void percentages. The highest localised void percentage (19%) is detected in the Hy-SMCs (4 mm) specimen and is spotted at the interface of the UD fibre layer and randomly oriented fibre core. This may be attributed to low compression pressure as the process settings were optimised for a 2 mm thick specimen. Similarly, the top sectional localised void percentage of 9.5 and 5.1% is detected in 4 and 3.4 mm thick SMCs, respectively, and may have been influenced by upper tool-buckling during transfer and consolidation. Furthermore, voids and defects such as fibre undulation and matrix/fibre-rich zones are inevitable, and there is an inverse trade-off between composite part thickness and processing conditions like pressure and temperature.

Table 5. The void volume fraction of SMCs and Hy-SMCs specimens with the corresponding thickness (t).

Specimen	Void content [vol%]
SMCs (2 mm)	0
SMCs (3.4 mm)	1.3
SMCs (4 mm)	1.1
Hy-SMCs (3.4 mm)	0
Hy-SMCs (4 mm)	1.3

3.2. ILSS and HDT

The ILSS and heat deflection under constant load at elevated temperatures are necessary to assess the quality of the compression moulded SMC plates. The objectivity of ILSS evaluation is to minimise the influence of flexural responses (compressive and tension stress) and maximise the induced shear stresses due to the relatively low span-to-thickness ratio [27]. The ILSS also depends on the integrity and fabrication quality of SMCs parts, hence it is well suited to evaluate the impact of selected processing parameters. In Figure 8, the applied axial load is line plotted against the recorded displacement of SMCs (2 mm) specimens, and the averaged recorded maximum load and the corresponding displacement (0.9±0.2 mm) is indicated by a marker with error bars. As a result, the mean interlaminar shear strength and error with a 95% confidence interval (CI) of pressed SMCs (2 mm) is assessed to

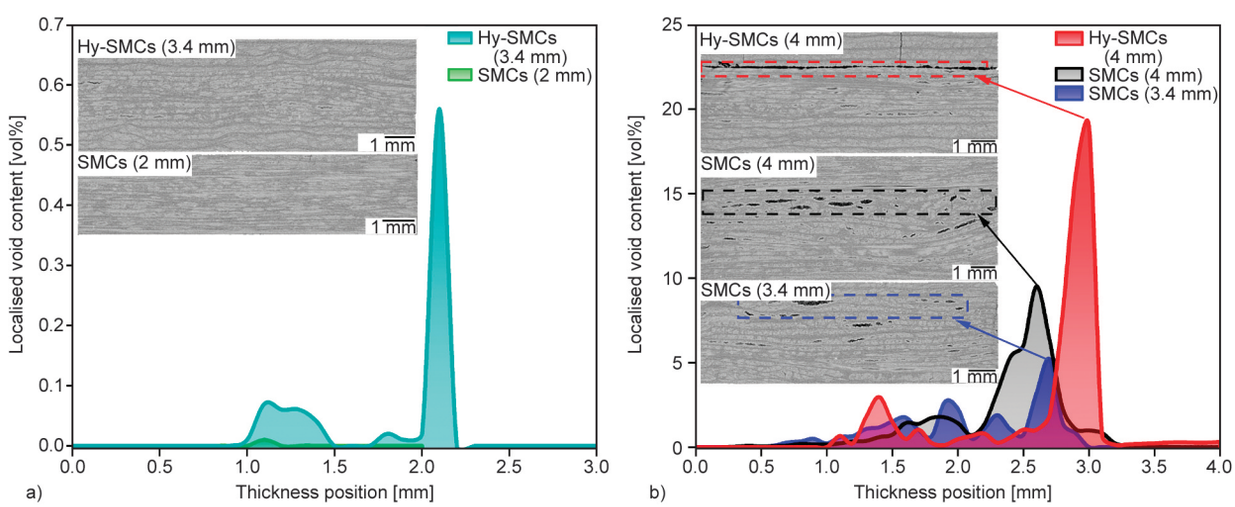

Figure 7. Localised void content of a) samples Hy-SMCs (3.4 mm) and SMCs (2 mm) and b) samples Hy-SMCs (4 mm), SMCs (4 mm) and SMCs (3.4 mm) over the individual specimen thickness, with corresponding sectional XCT images with markings of the highest localised void region.

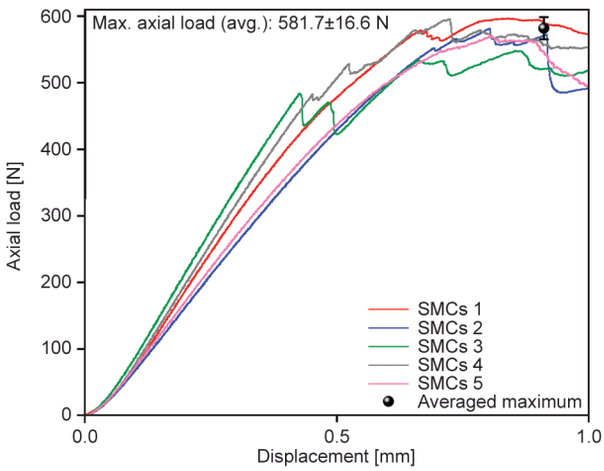

Figure 8. Resulting axial load *vs*. displacement curves of SMCs (2 mm) from ILSS experiments. The averaged maximum axial load is indicated by marker and error bars (CI 95%).

34.1±1 MPa with a coefficient of variation (CoV) of 3.8%. Similarly, the recorded maximum load endured by the SMCs specimen is 581.7±16.6 N at 3.8% of CoV. The multi-shear peak maxima are not appreciated nor accepted in the UD composites, but in SMCs, it is a consequence of the stacked randomised fibre orientation.

Only mid-plane interlaminar shear failure (MP-ILSF) specimens were evaluated to determine the ILSS due to the false apparent value resulting from tensile and compressive failures in SMCs subjected to transverse loading. Due to the nature of SMCs, we observed tension failure (TF), compressive failure (CF), interlaminar shear failure (ILSF) and MP-ILSF. The digital photography of fractured SMCs (2 mm) with different failure types is descriptively shown in Figure 9. Indicatively, in Figure 9a, a typical mid-plane interlaminar shear failure is shown with a red pointed arrow and a combination of MP-ILSF and ILSF is shown in Figure 9b. Similarly, TF and CF are shown in Figure 9c and Figure 9d.

The measured displacement is plotted against temperature in Figure 10. Initially, there is negative deflection for all samples, and it continued till 140 °C in HDT-B and up to 130 °C in HDT-C test conditions. In Figure 10, the negative deflection in composites resulted from thermal dilatation, causing the composite material to deflect opposite to the applied load due to the support pins, similarly reported by Li and Mason [12]. Furthermore, the increased constant test load in HDT-C (8 MPa) compared to HDT-B (0.45 MPa) mode negatively influenced the measured temperature at the highest deflection regardless of specimen types. Conversely, at constant low load conditions (HDT-B), the measured value shifted to a higher temperature, indicating load-depended amorphous PC matrix material response. Interestingly, in HDT-C, the recorded deflection with corresponding temperature similarly follows the phase transition thermogram between 125 to 145 °C, the glass transition temperature range of consolidated PC SMCs measured in differential scanning calorimetry (inset). Moreover, the measured temperature at the highest deflection for SMCs and Hy-SMCs in HDT-C type test condition is approximately 138.1±0.1 and 138.3±1 °C, respectively. Also, the measured temperature at the highest deflection in HDT-B mode for SMCs is 155±0.1 °C, and for Hy-SMCs is 160±0.7 °C. The significant increase in measured HDT for Hy-SMCs in HDT-B mode may be due to resistance to deflection by unidirectional fibres (out-of-plane aligned to applied load) reinforced in the top and bottom surface.

3.3. Dynamic mechanical thermal analysis (DMTA)

In Figure 11, the thermo-mechanical response graph, storage modulus, E' (solid line) and the loss angle tangent, tan δ (dotted line), were obtained as a function of temperature. The glass transition temperature (T_g) is evaluated by locating the onset and inflexion point in storage modulus and peak maxima in tan δ curves. The T_g onset indicates the rapid decrease of the material´s storage modulus, leading to a reduced mechanical performance at elevated temperatures. Similarly, the damping characteristics of composite materials and historical DMTA-determined T_g reference values are based on the tan δ peaks. Moreover, T_g in amorphous PC phase transition during heating is not influenced by long/continuous fibrous materials reinforcement. Independent of composite type and thickness, PC matrix material T_g values are evaluated at 148–153 °C (E' onset), and with strong loss angle tangent apex at 171–173 °C (tan δ peak). Furthermore, the determined T_g value of materials in DMTA can range to a difference of 25 °C based on the chosen methodology [28–30]. The E' is indicative of the elastic response of the material, and the value at the onset of T_g is a significant indicator of composite part performance that is subjected to temperature and load. The storage modulus of SMCs (3.4 mm), SMCs (2 mm) and Hy-SMCs (3.4 mm) at the onset of T_g is 14.3±0.6, 16.3 ±1.3 and 22.7±1 GPa,

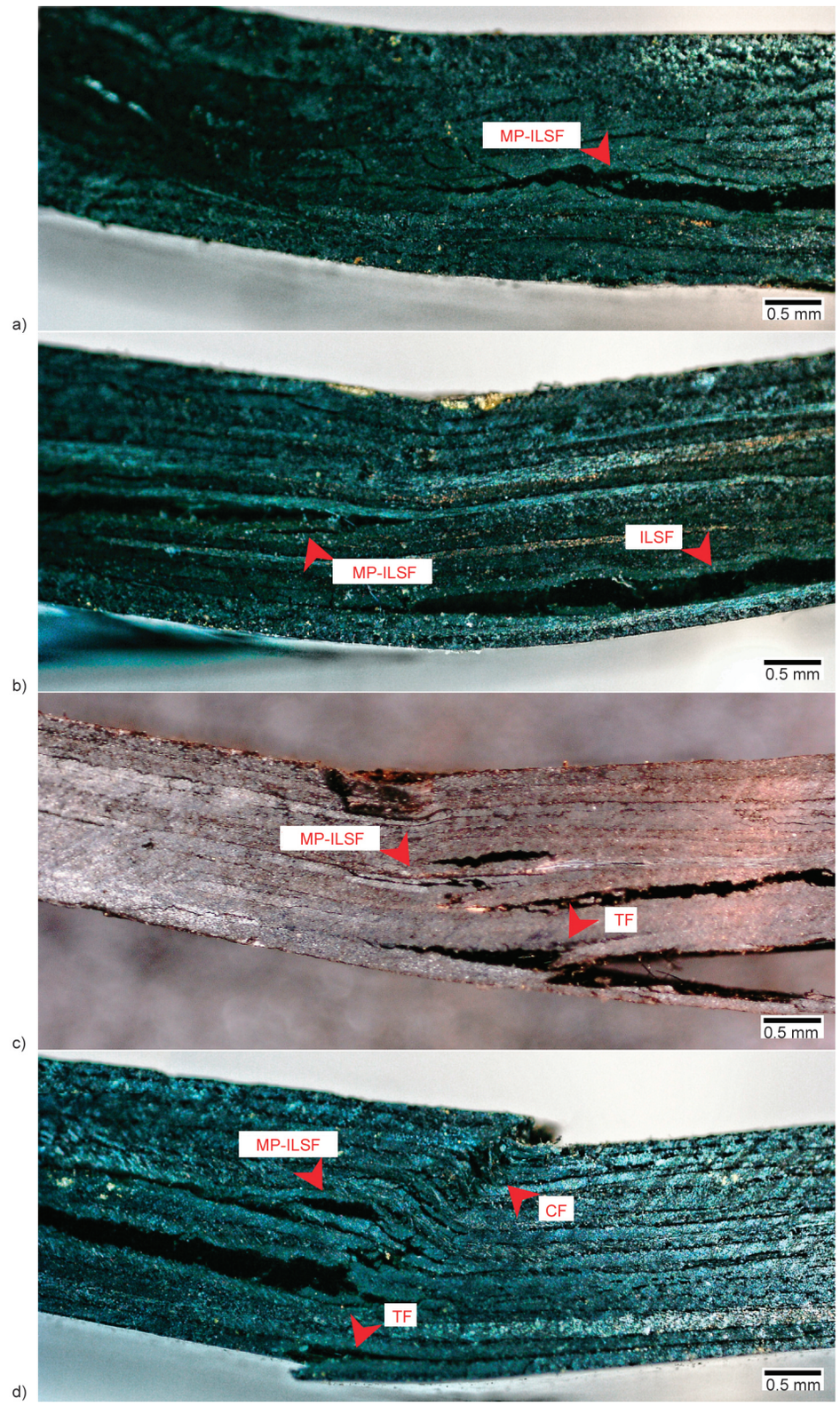

Figure 9. ILSS tests fractured SMCs (2 mm) specimens with different failure types. a) and b) Image highlights the midpoint interlaminar shear failure (MP ILSF) and interlaminar shear failure (ILSF); c) and d) image showcases a kinked specimen with combined tension failure (TF), compressive failure (CF) and MP-ILSF.

respectively. Researchers Kore *et al.* [13] reported similar thermomechanical properties for continuous biaxial fabric (±45°) composite (3.5 mm thick) specimens. This finding suggests that repurposed SMCs and Hy-SMCs may possess material properties that are equivalent-to bidirectional composite parts. The higher modulus of Hy-SMCs (3.4 mm) at the onset temperature compared to SMCs (3.4 mm) may be

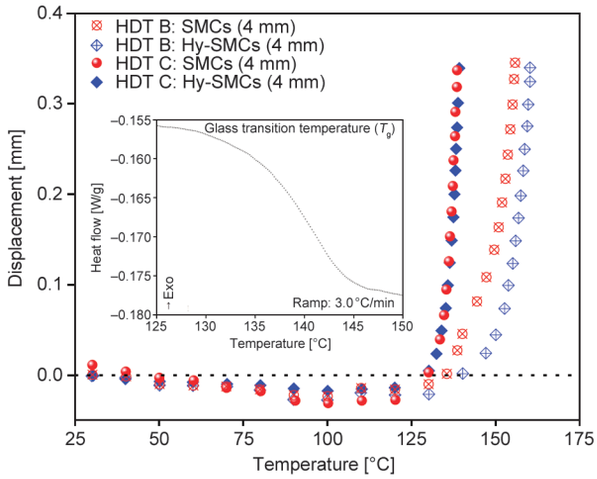

Figure 10. Recorded Heat deflection temperature *vs.* displacement of SMCs and Hy-SMCs, inset represents DSC thermogram of consolidated UD-tape. The straight dotted line indicates zero displacement.

attributed to UD carbon fibre reinforcement. Interestingly, only in Hy-SMCs (3.4 mm), an increase in E' (3.5%) before the onset of T_g was observed in a viscoelastic curve due to apparent stiffening of the reinforced UD carbon fibre composite. The SMCs (2 mm) specimen shows better resistance to deformation under load and temperature compared to SMCs (3.4 mm), indicative of optimised fabrication processing settings. Similarly, there is a noticeable difference between SMC specimens in terms of tan δ absolute value; SMCs (3.4 mm) have higher loss angle tangent response at all temperatures.

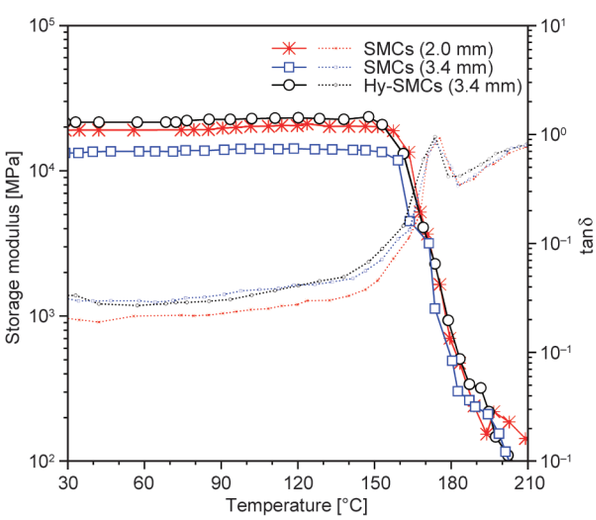

Figure 11. The three-point bending thermo-mechanical plot, storage modulus, E' (solid line) and loss tangent, tan δ (short dot line) data at 1 Hz are plotted as functions of temperature.

3.4. Notched Charpy impact test

Summarised notched Charpy impact tested data of SMCs (4 mm) and Hy-SMCs (4 mm) are tabulated in Table 6. SMCs and Hy-SMCs have similar impact values and are within the 95% CI error for both specimen types. Nevertheless, SMCs (4 mm) and Hy-SMCs (4 mm) have high notched Charpy impact strength of 101.7±10.1 and 108±14.5 kJ·m^{-2}. However, the high CoV of Hy-SMCs and SMCs may be attributable to previously observed void formation at the interface of UD tapes and core and in the core section, respectively (see Figure 6). Additionally, remarkable fibrillations are observed in the impacted tested SMCs compared to Hy-SMCs specimens (see Figure 12), which was also observed in fractographic images (Figure 13), and it is due to randomised fibre orientation. Also, the overall increased notch sensitivity of out-of-plane fibre orientations in SMCs and Hy-SMCs has negatively influenced the impact property with high CoV. The inefficient load transfer between the TP matrix and carbon fibres is leading to fibre matrix debonding, as shown in Figure 13 SMCs.

The fractography of notched Charpy impact tested SMCs, and Hy-SMCs specimen is descriptively shown in Figure 13 using SEM at different spatial resolutions. The major complications in understanding the SMCs fractography are the strong interactions developed between the different fracture modes. One such example is in-plane shear failure in multi-directional laminates and is characterised by stepped translaminar fractures in highly-anisotropic fibre orientation (0°). This is evidently shown in Figure 13 SMCs (Figure 13a) and Hy-SMCs (Figure 13d, and Figure 13e). Additionally, the influences of voids can be apparent on the fracture surfaces like loose fibres, and negative or vacant space at the junction of randomly oriented fibres, as shown in SMCs and Hy-SMCs. Interestingly, both specimen types exhibit ductile matrix failure in the intersection of in-plane

Table 6. The results of the hy-SMCs and SMCs specimens' Charpy notch impact tested were.

Specimen	Statistics	Notched impact strength [kJ·m^{-2}]
SMCs (4 mm)	Average	101.7
	CoV	13.3
	Error (95% CI)	10.1
Hy-SMCs (4 mm)	Average	108.0
	CoV	20.2
	Error (95% CI)	14.5

and out-of-plane oriented carbon fibres and simultaneously a brittle matrix failure at the in-plane oriented fibres. Henceforth, fractographic analysis is essential in gaining insight into such complex interactions.

Figure 12. Photographic image of notched Charpy impacted tested SMCs, and the red arrow in Hy-SMCs indicate fibre direction in Hy-SMCs specimens.

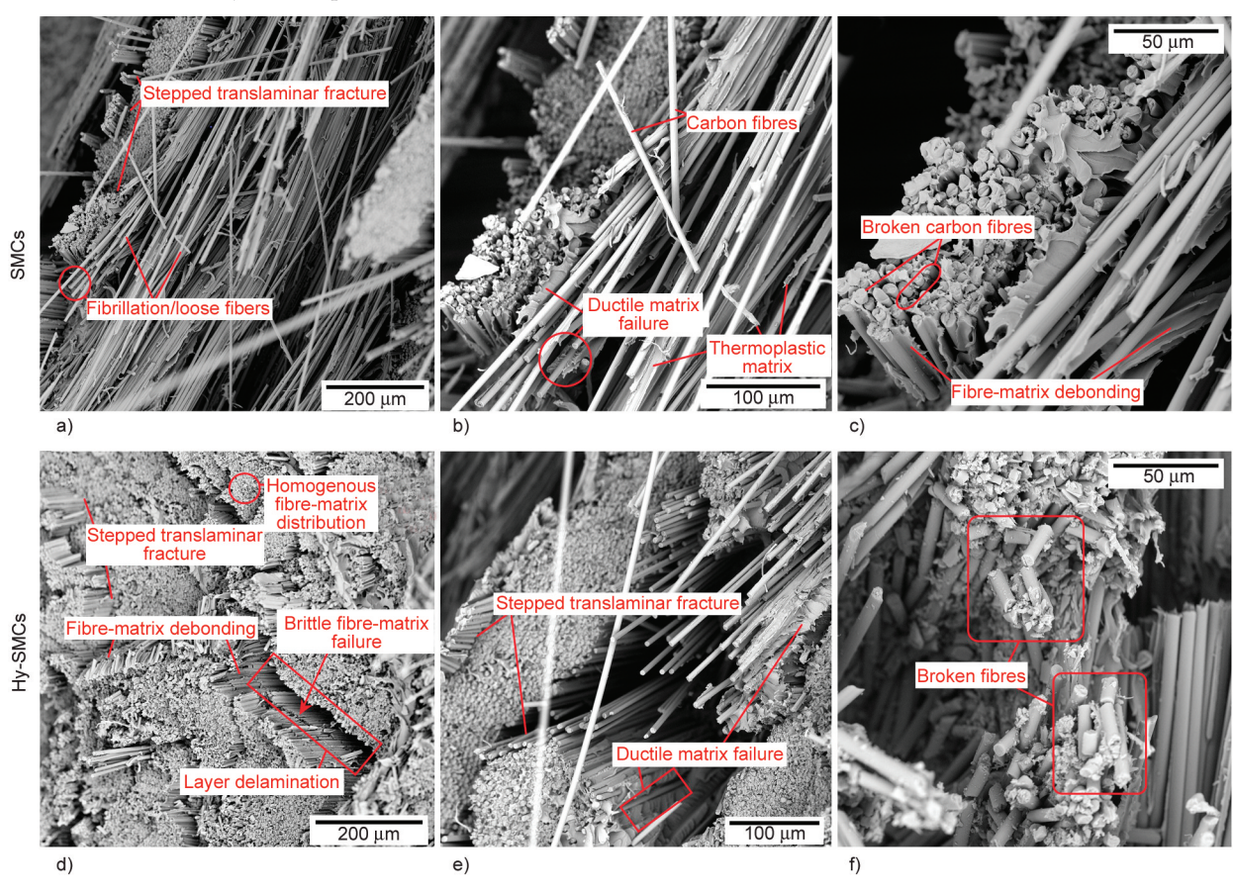

Figure 13. Fractographic images of Charpy impacted tested SMCs and Hy-SMCs using scanning electron microscope with different spatial resolution. The investigative markings represent the distinct fracture behaviour within the SMCs and Hy-SMCs. Image a) gives an overview of fractured surface of SMCs, b) shows region of interest (ROI) at better resoultion, and c) shows ROI at higher resoultion. Similarly Hy-SMCs d) shows an overview of fractured surface, e) and f) shows ROI at different resolution.

3.5. Tensile and flexural

The tensile strength (σ_t), tensile modulus (E_t) and flexural strength (σ_f), flexural modulus (E_f) are tabulated in Table 7 along with referenced general-purpose aluminium material properties. The thermo-mechanical performance of the carbon fibre-reinforced conventional TP composite is always dependent on the fibre orientation, *i.e.*, resistance to load and performance metrics are high in fibre direction compared to transverse or out-of-plane fibre orientation. Like previous report by Belliveau *et al*. [22], the applied flexural loading on the randomised fibre oriented SMCs led to local weaknesses due to the in-plane highly anisotropic mechanical properties of the platelets. It is evident that flow induced fibre re-orientation (see Figure 6 SMCs) lead to anisotropic material behaviour in SMCs (4 mm) with different tensile to flexural values, similarly reported in [31]. Also, the different initial slope (see Figure 14) in flexural tested SMCs may be attributed to highly randomised fibre reorientation compared to Hy-SMCs. Conversely, the introduction of UD tapes in 50:50 ratio accomplished an increased mechanical strength to weight ratio compared to generic aluminium grade shown in Table 7. The Hy-SMCs (4 mm) has approximately similar tensile (σ_t = 563.6±91.1 MPa and E_t = 65.8±11.2 GPa) and flexural material properties (σ_f = 550.3±39.1 MPa and E_t = 67.2±6 GPa). The repurposed SMCs and Hy-SMCs had similar flexural strength and modulus compared to PC-based non-crimp fabric and UD composite plates reported by Shinohara *et al*. [32] and Kore *et al*. [13].

Figure 14 showcases a typically stress-strain behaviour of SMCs and Hy-SMCs subjected to flexural 4PB loading. Hy-SMCs exhibit stiffer, stronger responses than SMCs, with both showing nonlinear flexural fracture behaviour. The use of UD tapes proved beneficial for tensile and flexural loading in Hy-SMCs (4 mm), with approximately 81–85% increase in mechanical strength compared to generic aluminium grade.

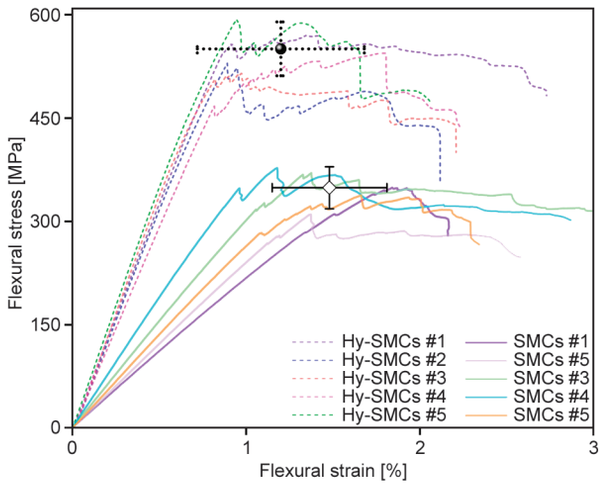

Figure 14. Stress-strain graph of flexural tested 4 mm thick specimens of Hy-SMCs and SMCs. The markers represent respective averaged flexural strength and averaged strain at flexural strength with corresponding error bars (95% CI).

The distinct tensile tested fracture behaviour owing to the nature of the composite are descriptively shown as cross-sectional images using XCT in Figure 15. It is difficult to detect the crack initiation in SMCs during tensile testing, but according to Belliveau *et al*. [25], the crack propagates between the interface of several out-of-plan platelets subjected to tensile load (in the plane). In XCT sectional image of tensile tested SMCs specimen (Figure 15), we observed broken, split and pulled out platelets including tow undulation, such complex failure with combined failure modes (Table 8) were similarly observed by Howell and Fukumoto [1]. Conversely, in Hy-SMCs, tensile fractured behaviour follows typical in-plane-oriented UD composites, dominated by jagged teeth like a failure, split-pulled-out platelets, and broken tows due to slight undulation in UD tapes after consolidation (see Figure 6).

Similarly, we observed three types of failure modes in 4PB fractured specimens in SMCs, such as

Table 7. Tensile and flexural of SMCs, Hy-SMCs, and a reference generic grade aluminium property. The composite's tensile and flexural data are evaluated to 95% CI.

Material properties	Unit	Aluminium (6061-T6) [1]	SMCs	Hy-SMCs
Density	g·cm^{-3}	2.7	1.5	1.5
Tensile strength, σ_t	MPa	303.0±44.0	244.6±59.7	563.6±91.1
Tensile modulus, E_t	GPa	69.0±10.0	43.4±11.9	65.8±11.2
Flexural strength, σ_f	MPa	303.0±44.0	348.9±30.5	550.3±39.1
Flexural modulus, E_f	GPa	69.0±10.0	28.7±7.6	67.2±6.0

Table 8. Tensile tested specimens' failure codes of SMCs and Hy-SMCs (3.4 mm).

Specimen number		**SMCs**		**Hy-SMCs**	
1		MWT		MGM	
2		MAT		MIT	
3		MGT		MGM	
4		MWT		MGB	
5		MAB		MGB	
First character		**Second character**		**Third character**	
Failure type	**Code**	**Failure area**	**Code**	**Failure location**	**Code**
Multimode	M	1<W from grip/tab	W	Top	T
		At grip/tab	A	Bottom	B
		Gauge	G	Middle	M
		Inside grip/tab	I		

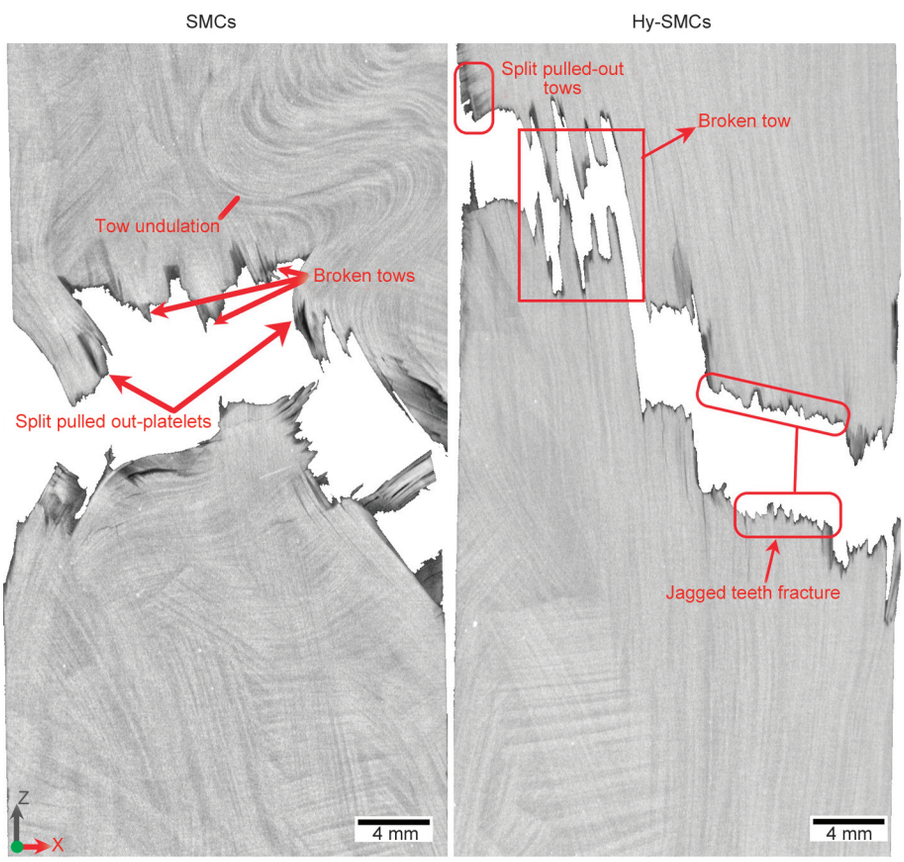

Figure 15. XCT two-dimensional rendering of tensile tested specimens showing distinct fracture behaviour, and the tensile force is in the z-axis direction.

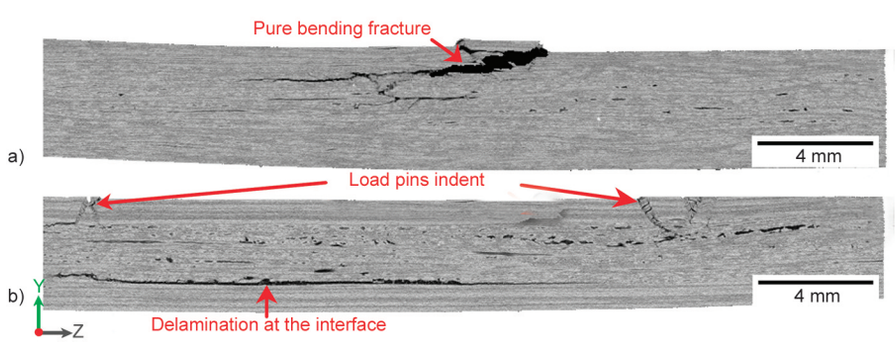

Figure 16. X-ray computed tomography image of 4-point bending flexural tested SMCs (a) and Hy-SMCs (b) with different fracture behaviour.

tension side cracking and compression failure, combined with interlaminar failure (See Figure 16). Additionally, Hy SMC tension side cracking along with compression failure with interlaminar failure at the junction of SMCs and UD tapes. The interlaminar failure may originate from bonding weaknesses and voids observed (refer to Figure 7) between randomly oriented platelets and UD tapes. Importantly, this failure does not confine itself to the original defect layer; instead, it propagates until it reaches a 'preferential' platelet interface.

4. Conclusions

The investigation into the thermo-mechanical properties of Hy-SMCs and SMCs has provided comprehensive insights into the influence of fabrication quality and material composition on their performance. Through advanced non-destructive imaging techniques such as XCT, it has been demonstrated that the orientation and the processing quality of fabricated composites significantly affect the overall integrity and thermo-mechanical properties. The void volume fraction analysis highlights that optimised fabrication processes can minimise void content for thinner SMCs compared to thicker SMCs. Furthermore, the DMTA further elucidates the thermal properties, showing a clear correlation between fibre reinforcement and thermal stability, with Hy-SMCs demonstrating superior performance due to unidirectional carbon fibre reinforcement. The mechanical testing, including tensile, flexural, and impact tests, underscores the complex interplay between fibre orientation, void content, and material behaviour under stress. The notched Charpy impact test results indicate that while SMCs and Hy-SMCs have comparable impact strengths, the presence of voids and fibre orientation can significantly affect the impact resistance and fracture behaviour. Further research should focus on refining fabrication techniques to achieve even better material uniformity and performance consistency. Optimising consolidation conditions and redesigning the SMCs to UD tape ratio may enhance the thermo-mechanical performance of Hy-SMCs. In conclusion, the study underscores the importance of controlled fabrication processes in optimising the thermo-mechanical properties of SMCs and Hy-SMCs. The findings pave the way for improved design and manufacturing strategies, enhancing the applicability of these composite materials in various industrial applications. This includes automotive parts such as high-performance motor and battery enclosures, motorcycle helmets, and connecting rods.

Acknowledgements

Humble thanks to Eva Kobler, János Géza Birtha, Fabio Uebelhoer, Micheal Lackner and Juergen Lesslhumer for facilitating the experimental setups. We acknowledge financial support for the COMET Centre CHASE (Funding period 2: 901897), REUSE (Interreg SI-AT), and sustaiNDT (grant nr. 909801), funded within the framework of the COMET Competence Centres for Excellent Technologies by Federal Ministry of Climate Action, Environment, Energy, Mobility, Innovation and Technology (BMVIT), Federal Ministry for Digital and Economic Affairs (BMDW), the Federal Provinces of Upper Austria, Vienna and Carinthia, European Regional Development Fund (ERDF), Carinthian Economic Development Fund (KWF), Austrian Research Promotion Agency (FFG).

References

[1] Howell D. D., Fukumoto S.: Compression molding of long chopped fiber thermoplastic composites. in 'CAMX 2014 – Composites and Advanced Materials Expo, Orlando, USA' CX1-47710 (2014).

[2] Kiss P., Stadlbauer W., Burgstaller C., Stadler H., Fehringer S., Haeuserer F., Archodoulaki V-M.: In-house recycling of carbon- and glass fibre-reinforced thermoplastic composite laminate waste into high-performance sheet materials. Composites Part A: Applied Science and Manufacturing, **139**, 106110 (2020). https://doi.org/10.1016/j.compositesa.2020.106110

[3] Fitzgerald A. M., Wong N., Fitzgerald A. V. L., Jesson D. A., Martin F., Murphy R. J., Young T., Hamerton I., Longana M. L.: Life cycle assessment of the high performance discontinuous fibre (HiPerDif) technology and its operation in various countries. Sustainability, **14**, 1922 (2022). https://doi.org/10.3390/su14031922

[4] Stelzer P. S., Cakmak U., Eisner L., Doppelbauer L. K., Kállai I., Schweizer G., Prammer H. K., Major Z.: Experimental feasibility and environmental impacts of compression molded discontinuous carbon fiber composites with opportuni ties for circular economy. Composites Part B: Engineering, **234**, 109638 (2022). https://doi.org/10.1016/j.compositesb.2022.109638

[5] la Rosa A. D., Cozzo G., Latteri A., Mancini G., Recca A., Cicala G.: A comparative life cycle assessment of a composite component for automotive. Chemical Engineering Transactions, **32**, 1723–1728 (2013). https://doi.org/10.3303/CET1332288

[6] la Rosa A. D., Cicala G.: LCA of fibre-reinforced composites. in 'Handbook of life cycle assessment (LCA) of textiles and clothing' (ed.: Muthu S. S.) Elsevier, Sawston, 301–323 (2015). https://doi.org/10.1016/B978-0-08-100169-1.00014-9

[7] Eguémann N., Giger L., Dransfeld C., Thiebaud F., Perreux D.: Compression moulding of complex parts for the aerospace with discontinuous novel and recycled thermoplastic composite materials. in 'Proceeding of the 19th International Conference on Composite Materials, Montréal, Canada' hal-00983314 (2013).

[8] Eguémann N., Giger L., Masania K., Dransfeld C., Thiebaud F., Perreux D.: Processing of characterisation of carbon fibre-reinforced PEEK with discontinuous architecture. in 'Proceeding of the ECCM16-16th European Conference on Composite Materials, Seville, Spain' SETEC-8199 (2014).

[9] Roux M., Dransfeld C., Eguémann N., Giger L.: Processing and recycling of a thermoplastic composite fibre/PEEK aerospace part. in 'Proceeding of the ECCM16-16th European Conference on Composite Materials. Seville, Spain' SETEC-8183 (2014).

[10] Bernatas R., Dagreou S., Despax-Ferreres A., Barasinski A.: Recycling of fiber reinforced composites with a focus on thermoplastic composites. Cleaner Engineering and Technology, **5**, 100272 (2021). https://doi.org/10.1016/j.clet.2021.100272

[11] Trauth A., Weidenmann K. A.: Continuous-discontinuous sheet moulding compounds – Effect of hybridisation on mechanical material properties. Composite Structures, **202**, 1087–1098 (2018). https://doi.org/10.1016/j.compstruct.2018.05.048

[12] Li X., Mason J.: New perspective on heat deflection temperature of glassy polycarbonate. Macromolecular Materials and Engineering, **294**, 306–314 (2009). https://doi.org/10.1002/mame.200800334

[13] Kore S., Murthy V. S. M. D., Hiremath N., Theodore M., Young S., Penumadu D., Vaidya U.: Textile-grade carbon fiber-reinforced polycarbonate composites: Effect of epoxy sizing. Industrial and Engineering Chemistry Research, **60**, 3981–3991 (2021). https://doi.org/10.1021/acs.iecr.0c05724

[14] Selezneva M., Lessard L.: Characterization of mechanical properties of randomly oriented strand thermoplastic composites. Journal of Composite Materials, **50**, 2833–2851 (2016). https://doi.org/10.1177/0021998315613129

[15] Selezneva M., Roy S., Meldrum S., Lessard L., Yousefpour A.: Modelling of mechanical properties of randomly oriented strand thermoplastic composites. Journal of Composite Materials, **51**, 831–845 (2017). https://doi.org/10.1177/0021998316654748

[16] Birtha J., Marschik C., Kobler E., Straka K., Steinbichler G., Schlecht S., Zwicklhuber P.: Optimizing the process of spot welding of polycarbonate-matrix-based unidirectional (UD) thermoplastic composite tapes. Polymers, **15**, 2182 (2023). https://doi.org/10.3390/polym15092182

[17] Birtha J., Kobler E., Marschik C., Straka K., Steinbichler G.: Using heating and cooling presses in combination to optimize the consolidation process of polycarbonate-based unidirectional thermoplastic composite tapes. Polymers, **15**, 4500 (2023). https://doi.org/10.3390/polym15234500

[18] Kobler E., Birtha J., Marschik C., Straka K., Steinbichler G., Zwicklhuber P., Schlecht S.: A novel multi-region, multi-phase, multi-component-mixture modeling approach to predicting the thermodynamic behaviour of thermoplastic composites during the consolidation process. Polymers, **14**, 4785 (2022). https://doi.org/10.3390/polym14214785

[19] Stelzer P. S., Plank B., Major Z.: Mesostructural simulation of discontinuous prepreg platelet based carbon fibre sheet moulding compounds informed by X-ray computed tomography. Nondestructive Testing and Evaluation, **35**, 342–358 (2020). https://doi.org/10.1080/10589759.2020.1774584

[20] Plank B., Sause M. G. R., Kastner J.: High-resolution X-ray computed tomography simulations of synthetically-generated volume porosity in continuous carbon fibre-reinforced polymer samples. Nondestructive Testing and Evaluation, **37**, 645–665 (2022). https://doi.org/10.1080/10589759.2022.2086547

[21] Plank B., Rao G., Kastner J.: Evaluation of CFRP-reference samples for porosity made by drilling and comparison with industrial porosity samples by means of quantitative X-ray computed tomography. in 'Proceeding of the 7th International Symposium on NDT in Aerospace. Bremen, Germany' 18926 (2015).

[22] Belliveau R., Landry B., LaPlante G.: A 3D finite element model to simulate progressive damage in unidirectional- and woven-fibre thermoplastic discontinuous-long-fibre composites. Journal of Thermoplastic Composite Materials, **36**, 4669–4683 (2023). https://doi.org/10.1177/08927057231158535

[23] Martulli L. M., Creemers T., Schöberl E., Hale N., Kerschbaum M., Lomov S. V., Swolfs Y.: A thick-walled sheet moulding compound automotive component: Manufacturing and performance. Composites Part A: Applied Science and Manufacturing, **128**, 105688 (2020). https://doi.org/10.1016/j.compositesa.2019.105688

[24] Belliveau R., Léger É., Landry B., LaPlante G.: Measuring fibre orientation and predicting elastic properties of discontinuous long fibre thermoplastic composites. Journal of Composite Materials, **55**, 321–330 (2021). https://doi.org/10.1177/0021998320949635

[25] Belliveau R., Landry B., LaPlante G.: Comparative study of the mechanical properties of woven and unidirectional fibres in discontinuous long-fibre composites. Journal of Thermoplastic Composite Materials, **36**, 2372–2389 (2023). https://doi.org/10.1177/08927057221091084

[26] Tretiak I., Kawashita L. F., Hallett S. R.: Manufacturing composite laminates with controlled void content through process control. Journal of Reinforced Plastics and Composites, **43**, 16–29 (2024). https://doi.org/10.1177/07316844231154585

[27] Greene J. P.: Automotive plastics and composites: Materials and processing. William Andrew, Norwich (2021). https://doi.org/10.1016/C2018-0-03030-3

[28] Rudin A., Choi P.: The elements of polymer science and engineering. Elsevier, San Diego (2013).

[29] Yin S. P., Yu M.: Dynamic visco-elastic properties of polycarbonate (PC) under static and dynamic load. Advanced Materials Research, **146-147**, 1090–1093 (2010). https://doi.org/10.4028/www.scientific.net/AMR.146-147.1090

[30] Sehrawat M., Rani M., Bharadwaj S., Sharma S., Chauhan G. S., Dhakate S. R., Singh B. P.: Glass transition temperature measurement of polycarbonate specimen by dynamic mechanical analyser towards the development of reference material. MAPAN, **37**, 517–527 (2022). https://doi.org/10.1007/s12647-022-00572-3

[31] Feraboli P., Cleveland T., Ciccu M., Stickler P., DeOto L.: Defect and damage analysis of advanced discontinuous carbon/epoxy composite materials. Composites Part A: Applied Science and Manufacturing, **41**, 888–901 (2010). https://doi.org/10.1016/j.compositesa.2010.03.002

[32] Shinohara M., Isshiki S., Fukushima Y., Katayama T., Tanaka K.: Moulding of carbon fiber reinforced polycarbonate (CF/PC) using UD tape. in 'Proceeding of the HPSM2012. Lisbon, Portugal' 249–257 (2012). https://doi.org/10.2495/HPSM120221